Ultrafast excited-state dynamics of a cyano-substituted "proton sponge"

Balkowski, G.; Szemik-Hojniak, A.; Buma, W.J.; Zhang, H.; Deperasińska, I.; Poisson, L.; Mestdagh, J.M.; Piani, G.; Oberda, K.

DOI
10.1021/acs.jpca.5b06631

Publication date
2015

Document Version
Final published version

Published in
The Journal of Physical Chemistry. A

THE JOURNAL OF PHYSICAL CHEMISTRY A

Article

pubs.acs.org/JPCA

Ultrafast Excited-State Dynamics of a Cyano-Substituted "Proton Sponge"

Grzegorz Balkowski,[†] Anna Szemik-Hojniak,*[,‡] Wybren Jan Buma,[†] Hong Zhang,[†] Irena Deperasińska,[§] Lionell Poisson,[∥,⊥] Jean Michel Mestdagh,[∥,⊥] Giovanni Piani,[∥,⊥] and Krzysztof Oberda[‡]

[†]Van't Hoff Institute for Molecular Sciences, University of Amsterdam, P.O. Box 94157, Science Park 904, 1098 XH Amsterdam, The Netherlands

[‡]Faculty of Chemistry, University of Wroclaw, 14 Joliot-Curie Str., 50-383 Wroclaw, Poland

[§]Institute of Physics, Polish Academy of Sciences, Al. Lotników 32/46, 02-668 Warsaw, Poland

[∥]CNRS, IRAMIS, LIDyL, and [⊥]CEA, IRAMIS, LIDyL, Laboratoire Francis Perrin (LFP), URA 2453, 91191 Gif-sur-Yvette, France

Supporting Information

ABSTRACT: The dynamics of a substituted proton sponge—the 1,8-bis(dimethylamino)-4-cyanonaphthalene (DMAN-CN) molecule—was investigated after excitation in the S_1 state. Experimental and theoretical information are reported. The former includes absorption, fluorescence, and time-resolved transient absorption spectra, which were recorded in solution. Real-time dynamics measurements were also performed on gas-phase isolated DMAN-CN. TD DFT/6-31G(d,p) level and CIS/6-31G(d,p) excited-state calculations complement these results. This has allowed revisiting the energy transfer process between a locally excited (LE) and a charge transfer (CT) state, which is often invoked with this kind of molecule.

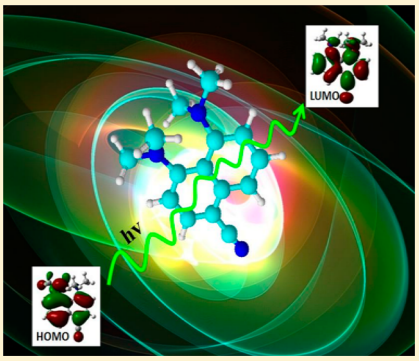

1. INTRODUCTION

After Lippert's discovery of dual fluorescence phenomenon in 1961 in dimethylaminobenzonitrile (DMABN),[1] the issue of electron transfer in excited donor−acceptor (D−A) systems became the subject of an ongoing interest. Many cases were reported in the gas phase, in solution, and in the solid state where the rotation of the donor group leads to the presence of the long wavelength emission band.[2−4] It is assumed that the twisted perpendicular conformation results in a charge transfer (CT) state which is responsible for the red emission. The blue emission band in those systems is ascribed to a weakly polar, locally excited state (LE). When an intramolecular hydrogen bond is present in the D−A systems, a more complicated phenomenon is at play: the proton-coupled electron transfer (PCET) process.[5] The proton and electron transfers may be concerted when they occur at about the same time. They can also be sequential with first the proton transfer and then the electron transfer (PET) or the reverse (EPT). These behaviors are ubiquitous in many chemical and naturally occurring systems, and recently they have intensively been studied from both experimental and theoretical points of view.[6] It has been shown that in some cases the directions of the proton and electron transfers can be totally different, while in some others both transfers take place in the same direction. Finally, the stepwise PET or EPT processes can occur between the same sites and with the same probability between different sites.[7] The processes that are mentioned above do not occur in natural systems only but also in areas of broad technological applications, such as nonlinear optics or the development of photovoltaic cells, light-emitting diodes (OLEDs), polarity probes, and many others.[8−10]

Molecules based on the 1,8-bis(dimethylamino)naphthalene skeleton belong to this category of compounds. They are named "proton sponges" because of their unusual basicity. They form a class of bicenter nitrogen bases that is attracting a large interest. The latter started in 1968 with the synthesis by Alder et al.[11] of the group precursor, the unsubstituted 1,8-bis(dimethylamino)naphthalene molecule (hereafter called DMAN). Shortly after, it was discovered that proton sponges originating from DMAN combine a strong basicity with a low nucleophilic character, paving the way for their use as auxiliary bases in organic synthesis.[12,13] More recently, proton sponges have also been used as matrices in MALDI-TOF experiments[14] and as proton receptors in fluorescent switches.[15]

From a spectroscopic point of view, proton sponges are very interesting as they exhibit charge transfer and undergo significant geometry changes in the excited state. In previous experiments[16,17] we studied the excited state manifold of unsubstituted DMAN using time-resolved transient absorption and fluorescence up-conversion techniques. These studies

Received: July 10, 2015
Revised: October 30, 2015
Published: October 31, 2015

DOI: 10.1021/acs.jpca.5b06631
J. Phys. Chem. A 2015, 119, 11233−11240

showed that initial excitation of the molecule to the "bright" ^1L_a state is followed by a cascade of relaxation processes that populates the relaxed $l\pi^*$ state of charge-transfer (CT) nature which is responsible for a red-shifted emission (540 nm).[18] A striking features of the $l\pi^*$ state is that the molecule is subject to major geometry changes driven by the formation of a two-center, three-electron bond between the lone pair orbitals of the dimethylamino groups.

An interesting question arose from these studies: to what extent the photochemical and photophysical properties of the DMAN core can be steered by substituents. Works in this direction were performed on a cyano-substituted proton sponge, 1,8-bis(dimethylamino)-4-cyanonaphthalene (DMAN-CN) (see Figure 1), in a combined experimental and

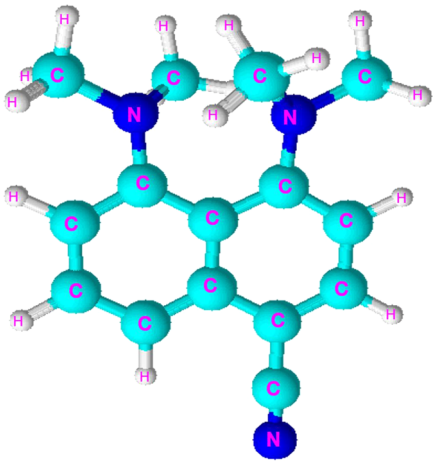

Figure 1. Molecular structure of 1,8-bis(dimethylamino)-4-cyano-naphthalene (DMAN-CN).

theoretical approach.[19,20] The computational results indicated an asymmetric CT character of the S_1 and the S_2 states resulting from the asymmetric location of the cyano group. It appeared that different contributions of electron density are transferred from both dimethylamino groups (DMA) to this strong CN electron acceptor. A satisfactory agreement is observed between experiment and calculation concerning the vertical excitation energies and oscillator strengths of the low-lying excited singlet states as well as the effect of solvatochromism.

As yet, however, only the steady-state spectroscopy of DMAN-CN has been investigated. In view of the concluded strong influence of the substituent on the DMAN core, it is of interest to investigate to what extent the photodynamics of the core is affected by such substitutions. This has motivated the present work, which reported a series of time-resolved spectroscopic studies both in solution and in the gas phase, complemented by quantum chemistry calculations.

2. EXPERIMENTAL AND CALCULATION METHODS

2.1. Synthesis. 1,8-Bis(dimethylamino)-4-CN-naphthalene (DMAN-CN) was obtained according to the procedure described elsewhere.[21] Its purity was checked by GC/MS.

2.2. Steady-State Spectroscopic Characterizations. *2.2a. Electronic Absorption Sspectra.* Steady-state absorption spectra were recorded using CARY-50 UV−vis (Varian) spectrometer. To collect them, a 10^{-5} M solution was prepared in *n*-hexane (Merck, used without any further purification).

2.2b. Fluorescence Spectra. Emission spectra were recorded on a PerkinElmer LS-50B fluorometer and on a FSL900 luminescence setup of Edinburgh Instruments Ltd. For excitation and emission spectra the optical density was kept at ∼0.2 (path length 1 cm) to avoid reabsorption and inner filter effects. Spectra were corrected for detector response and excitation source. The concentration of solutions was about 10^{-5} M. As the excitation source, a Xe900 (450 W) steady-state xenon lamp was employed. Fluorescence was detected using a red-sensitive (185−850 nm) single-photon counting photo-multiplier tube (R928-Hamamatsu) in a Peltier-cooled housing.

2.3. Time-Resolved Spectroscopy. *2.3a. Femtosecond Transient Absorption.* The setup for femtosecond transient absorption experiments in Amsterdam has been described in detail elsewhere.[22] Briefly, a 130 fs (fwhm) pulse train of spectral width of about 26 nm and centered at 800 nm is generated by a Spectra-Physics Hurricane regenerative amplifier laser system with a 1 kHz repetition rate. This pulse train is separated into two parts. One part pumps a Spectra-Physics OPA800 system to provide excitation pulses—in the present case at 350 nm—and the other part is focused on a calcium fluoride crystal to generate a white-light continuum from 350 to 800 nm which serves as the probe pulse. The total instrumental response is about 200 fs (fwhm). In the present experiments magic-angle conditions were employed for the pump and probe beam. Experiments were performed at ambient temperature on solutions with an absorbance of ca. 0.5 in a 1 mm cell. To avoid effects resulting from the high transient power radiation, the excitation power was kept as low as 5 μJ/pulse, and a pump spot diameter of about 1 mm was used. Apart from lowering the excitation intensity, the influence of thermal effects and possible photodegradation of the sample was taken care of by placing the circular cuvette containing the solution in a homemade ball-bearing (1000 rpm). Absorption and emission spectra were checked before and after experiments to exclude photochemical reaction have occurred. In order to illustrate properly both ultrafast (subpicosecond) and "slow" (hundreds of picoseconds) processes, we performed experiments with different time steps in each case (0.04 ps for the ultrafast time window and 40 ps for the long time window).

2.3b. Time-Correlated Single Photon Counting. Fluorescence decay curves were recorded using nanosecond time-correlated single photon counting (TCSPC) option of FSL920 setup (Edinburgh Instruments Ltd.) with LED as the excitation source. The excitation was done at 375 nm. Data acquisition ensured Plug-in PC Card Model TCC900 with maximum count rate 3 MHz, time channels per curve up to 4096, and minimum time per channel 610 fs. To detect the emission, the MiniRed (185−850 nm) single photon counting photo-multiplier was applied.

2.3c. Femtosecond Resonance-Enhanced MultiPhoton Ionization (REMPI). The experimental setup for the gas-phase experiments has also been described elsewhere.[23,24] It combines a pulsed supersonic beam with a time-of-flight mass spectrometer (TOF-MS) and a photoelectron photoion velocity map imaging spectrometer along the design of Eppink and Parker.[24] In the present experiment only the TOF-MS was used. This setup is coupled to the LUCA femtosecond laser of the Saclay Laser Interaction Center (the SLIC Laserlab facility) in order to perform femtosecond pump/probe experiments where the probe operates by multiphoton ionization. DMAN-CN was seeded in a supersonic beam as described in ref 23. To this purpose DMAN-CN was mixed with graphite, and the

DOI: 10.1021/acs.jpca.5b06631
J. Phys. Chem. A 2015, 119, 11233−11240

mixture was pressed in a hydraulic press under 15 bar pressure to form a tablet. The sample tablet was put in an oven mounted directly on the nozzle plate of a pulsed valve (Parker solenoid valve, formerly General Valve, Series 9, nozzle diameter 0.5 mm) and maintained at a temperature of 100 °C. As a result, a DMAN-CN vapor is generated which is picked up by a free expansion of helium through the nozzle (stagnation pressure, 2 bar). After extraction by a homemade 1 mm diameter conical skimmer placed at 30 mm from the oven orifice (1.5 mm diameter), the molecular beam entered the interaction chamber where it is crossed by the pump and probe laser beams. The pump laser wavelength was 266 nm (third harmonic of a femtosecond Ti:sapphire laser operated at ∼800 nm). The molecules were probed in a multiphoton ionization scheme at 800 nm, using the fundamental emission of the Ti:sapphire laser. The cross-correlation width of the pump and probe pulses was measured to be 70 fs. The pump and probe pulses are delayed in time by passing the probe beam through an adjustable delay line. The polarization of the pump and probe lasers is linear and set parallel. The ion signal was mass-analyzed using the TOF-MS, and the intensity of the desired mass peak was recorded as a function of the pump−probe delay.

2.4. Computational Methods. Ground-state optimization of DMAN-CN was performed using density functional theory at the B3LYP/6-31G(d,p) level, while the CIS/6-31G(d,p) method was employed for geometry optimization in the excited (S_1) state. Reasons for the latter choice is that excited state optimization at higher level are too consuming in terms of computer time. In contrast, the energy calculations at optimized geometries, that of the ground state S_0 and that of the excited state S_1, were performed at the TD-DFT/B3LYP/6-31G(d,p) level. All calculations were performed using the Gaussian 09W, Revision B.01, package of programs.[25]

3. RESULTS AND DISCUSSION

The steady-state measurements are presented and discussed first, then the time-resolved measurements, and finally the calculations.

3.1. Absorption Spectra. The absorption spectrum of DMAN-CN dissolved in *n*-hexane is shown in Figure 1S of the Supporting Information (curve b in red). It displays two bands. The low-energy one with maximum at about 363 nm (∼27 548 cm^{-1}) corresponds to the $S_0 \rightarrow S_1$ excitation. The overall shape of this spectrum resembles that of the unsubstituted proton sponge DMAN, which is also shown on the figure (curve a in black). Nevertheless, the red band in the latter has a maximum at about 340 nm, indicating a red-shift of about 1900 cm^{-1} of this band due to the presence of the CN group in DMAN-CN. Absorption spectra of DMAN-CN in two other solvents are shown in the same figure. They match almost exactly the spectrum observed in *n*-hexane although one solvent has a higher viscosity (dodecane; curve c in blue) and the other a higher polarity (diethyl ether; curve d in green) than *n*-hexane.

3.2. Fluorescence Spectra. Figure 2 shows that excitation of DMAN-CN in *n*-hexane at 390 nm gives rise to a dual fluorescence spectrum with two well-resolved emission bands peaking at 454 and 630 nm, respectively. As put below on an experimental basis, the high-energy band is attributed to emission from the LE state while the band at 630 nm is assigned to emission from the S_1 state after relaxation in the solvent to a configuration of strong CT character. For convenience, it is often said throughout the paper that this emission is due to a CT state.

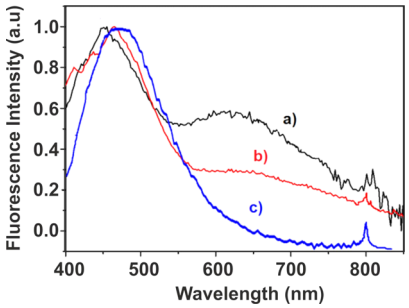

Figure 2. Normalized corrected fluorescence spectra of DMAN-CN recorded at room temperature in *n*-hexane (a), dodecane (b), and diethyl ether (c). The excitation wavelength was 390 nm.

The argument, which justifies that a state with strong CT character is responsible for the lower-lying emission, relies on the large Stokes shift of 13 500 cm^{-1} that is observed for this band in both *n*-hexane and dodecane. This value is indeed significantly larger than that measured for the DMAN molecule (12 000 cm^{-1}) in *n*-hexane,[17] hence suggesting a larger CT character in DMAN-CN than in DMAN. This is in line with the presence of the CN group in DMAN-CN, since this group is believed to be a strong electron attractor. The two solvents, *n*-hexane and dodecane, are weakly polar and have a similar dielectric permittivity of 1.89 and 2.0, respectively. This is consistent with the similarity between the broad low-energy bands which are observed in Figure 2 for these solvents (black and red curve, respectively). Of course, much larger Stokes shifts than 13 500 cm^{-1} are expected when DMAN-CN is dissolved in polar solvents. The fact that no low-lying emission band is observed with diethyl ether (ε = 4.33) in Figure 2 may appear surprising at a first glance. Actually, this substantiates somehow the assumption that a state with a strong CT character is present.

A very strong Stokes shift in this case can indeed either move the emission out of the observation window or move the CT state close enough to triplet states or even to the ground state (S_0) to turn on efficient nonradiative transfers and quench the fluorescence.

3.3. Transient Absorption Spectrum of the S_1 State at Long Time Delays (>40 ps). Here we address the excited-state photodynamics which is accessed upon excitation of the S_1 state at 350 nm. Figure 3 displays the transient absorption spectrum taken 40 ps after excitation of S_1 in an experiment

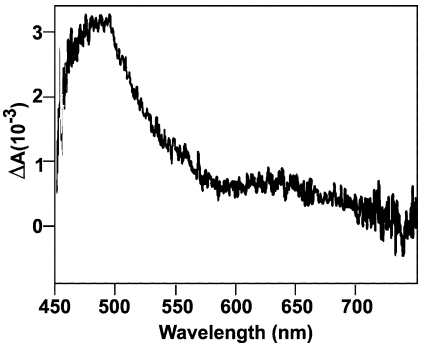

Figure 3. Transient absorption spectrum of the S_1 state of DMAN-CN in *n*-hexane, 40 ps after excitation of S_1 at 350 nm.

DOI: 10.1021/acs.jpca.5b06631
J. Phys. Chem. A 2015, 119, 11233−11240

where DMAN-CN is disolved in *n*-hexane. The spectrum is dominated by a band with apparent maximum at 490 nm, close to the blue side of the observation window. This band is heavily distorted since in this wavelength region also ground-state absorption starts to play a role as is indeed observed by the onset of a bleaching feature at lower wavelengths. Apart from this band, a much weaker and diffuse band is observed that covers the region from about 570 to 750 nm.

The shape of this spectrum does not change when it is recorded at longer delay times than 40 ps. However, its intensity decays. This suggests a similar decay behavior at all wavelengths. This has been checked directly by monitoring the transient absorption at specific wavelengths. One such decay is shown in Figure 4 when monitoring the transient absorption at

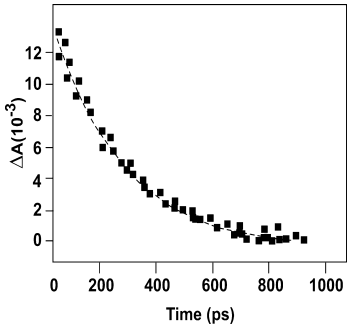

Figure 4. Observed signal decay when monitoring the transient absorption shown in Figure 3 at 490 nm as a function of time with time steps of 40 ps (squares).The fitted curve (black line) corresponds to a lifetime of 251 ± 5 ps.

490 nm. A monoexponential decay is observed which is nicely fitted with a decay time of 251 ± 5 ps. Of course, the fits performed at other wavelengths lead to very similar time constants, in agreement with the observation that no evolution of the spectrum occurs for delay times larger than 40 ps.

The presence of only one dominant component was further confirmed by singular value decomposition (SVD) analysis performed on the data matrix, which yielded only one component that could be unambiguously distinguished from the noise. This implies either that DMAN-CN follows monoexponential kinetics or that possible intermediates have a lifetime that is much shorter than the employed time step.

The above result meets the TC-SPC measurements of the emission shown in Figure 2S of the Supporting Information. There, DMAN-CN is excited at 375 nm in *n*-hexane, and the emission is monitored at 620 nm. The latter is fitted adequately by a single-exponential decay of 238 ± 8 ps time constant, after convolution with the instrumental response function. Similar values of 240 ± 10 and 250 ± 10 ps were obtained in diethyl ether and dodecane, respectively.

3.4. Transient Absorption Spectrum of the S_1 State at Short Time Delays (<40 ps). Figure 5 displays the time evolution of the transient absorption spectrum when the latter is monitored at 500 nm (curve a in blue), 620 nm (curve b in black), and 750 nm (curve c in red). The curves are normalized to put the decays in coincidence above 5 ps. In contrast with the observation at long time delays, a multiexponential behavior is observed that depends strongly on the observation wavelength. The 750 nm trace shows an ultrafast subpicosecond decay followed by a much slower decay, while at 500 nm an ultrafast growth is observed, again with a similar

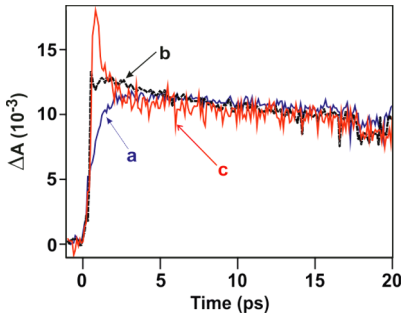

Figure 5. Time dependence of the normalized transient absorption traces of the S_1 state of DMAN-CN in *n*-hexane. The S_1 state was excited at 350 nm, and its absorption was monitored at 500 nm (curve a in blue), 620 nm (curve b in black), and 750 nm (curve c in red).

subpicosecond time constant. No such ultrafast component is observed at 620 nm although the rise time of the signal is extremely rapid and comparable to that observed at 750 nm. Clearly, the initial subpicosecond behavior is wavelength dependent, but after 3 ps, a monoexponential, wavelength independent decay is observed.

These results suggest that two dynamical processes of very different time scale are at play after excitation. To be quantitative, a global analysis of the decays in Figure 5 was performed using the Glotaran package.[26] Two decay processes with time constants of 620 ± 50 fs and 227 ± 10 ps are required to describe the observation. The latter time constant must be considered with caution since the time window of Figure 5 is limited to 20 ps. It is satisfactorily consistent with the decay time of 251 ± 5 ps determined in Figure 4 on a wider time windows. The latter value must be preferred.

Assuming that the two decay processes are sequential, their time constants reflect the lifetime of transient species which are populated sequentially after excitation of DMAN-CN at 350 nm in the S_1 state. That of short lifetime is likely associated with the absorption of S_1 in a geometry that departs only slightly from the Franck−Condon one, whereas that of long lifetime is likely associated with the absorption of equilibrated S_1 state after full geometrical and energetic relaxation with the solvent. The absorption spectra of the short-lived and long-lived species are shown in Figure 6. They were extracted for the global spectral analysis mentioned above.

3.5. Time-Resolved Studies on Gas Phase Isolated DMAN-CN. Time-resolved pump−probe studies of the excited-state dynamics of DMAN-CN isolated in the gas phase are reported in Figure 7. The probe operates by multiphoton ionization of DMAN-CN at 800 nm. The corresponding mass spectrum is shown in the inset of Figure 7. A single peak is observed at 239 Da, which is the mass of the parent molecule. Hence, the ionization does not lead to significant fragmentation, and for a full information on the dynamics, it is sufficient to record the intensity of the parent ion peak as a function of the delay time between the pump and probe pulses. The result is shown in Figure 7.

The signal is clearly multiexponential. It was fitted assuming a sequential $A \xrightarrow{\tau 1} B \xrightarrow{\tau 2} C \xrightarrow{\tau 3} D$ kinetic model, convoluted by a 70 fs width Gaussian function representing the cross-correlation between the pump and probe laser pulses. From these fits, the time constants of τ_1 = 100 ± 10 fs and τ_2 = 500 ± 50 fs were obtained. The "constant" signal observed at longer time delays in Figure 7 indicates that a third decay process may be present

DOI: 10.1021/acs.jpca.5b06631
J. Phys. Chem. A 2015, 119, 11233−11240

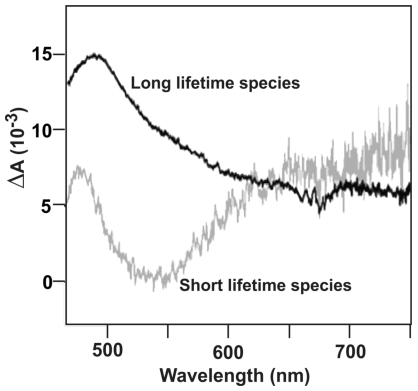

Figure 6. Absorption spectra of the transient species populated sequentially after excitation of DMAN-CN at 350 nm in *n*-hexane (see text for details). The gray trace is associated with the short-lived species (620 ± 50 fs lifetime) and the black trace with the long-lived species (251 ± 5 ps).

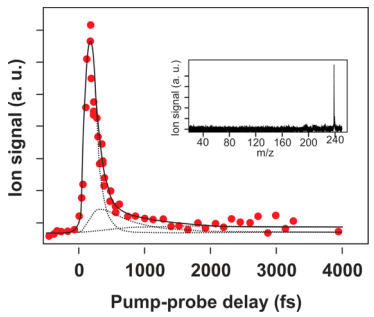

Figure 7. Ionization signal of DMAN-CN, at mass 239 Da, as a function of the pump (266 nm)−probe (800 nm) delay in the gas-phase isolation experiment. The experimental points are in red, and the solid line passing through is a fit, using the sequential $A \xrightarrow{\tau 1} B \xrightarrow{\tau 2} C \xrightarrow{\tau 3} D$ kinetic model discussed in the text. The components of the fit are reported as dotted and dashed lines. The inset with a single peak at mass 239 Da shows the time-of-flight mass spectrum of DMAN-CN provided by the multiphoton ionization at 800 nm.

but with a much longer time constant than 4 ps. Actually this signal has been followed experimentally up to 17.5 ps, and no significant decay was observed. Hence, the time constant τ_3 must be significantly longer than, say, 20 ps.

A likely interpretation of these results goes along the following scenario. The pump at 266 nm certainly populates an electronic state above S_1 which evolves very rapidly with the τ_1 = 100 ± 10 fs time constant to unrelaxed S_1. This is justified by the absorption spectrum shown in Figure 1S of the Supporting Information. Then, the wavepacket spreads on the S_1 surface with the time scale τ_2 = 500 ± 50 fs. The subsequent evolution out of the S_1 surface occurs with the very long time scale τ_3, which exceeds the time window of the experiment. Such a behavior, where a very rapid transfer to the S_1 is followed by a much slower relaxation, has been encountered in other organic compounds.[27] Interestingly, it has been shown also that when the wavepacket spreads on a S_1 surface, it may explore regions of very different electronic configurations.[28] This might be the case here, with regions of very different CT character on the S_1 surface.

3.6. Theoretical Calculations. The quantum chemistry calculations performed in the present work complement those of ref 19. The latter were focusing on permanent dipole moments and vertical excitation of the DMAN-CN molecule, whereas relaxed geometries in the S_1 state are considered also in the present work. Reference 9 showed that the ground-state dipole moment of 7.08 D increases substantially upon electronic excitation. At the geometry of the ground state, large dipole moments μ = 17.08, 13.67, and 16.80 D were calculated indeed for the S_1, S_2, and S_4 excited states, respectively. This suggests that the separation of charges is much larger in these states than in the ground state. The present calculations confirm this picture and extend it to the equilibrium geometry of the S_1 state. A summary of the new results appears in Figure 8, Table 1, and Figure 3S. They are detailed below.

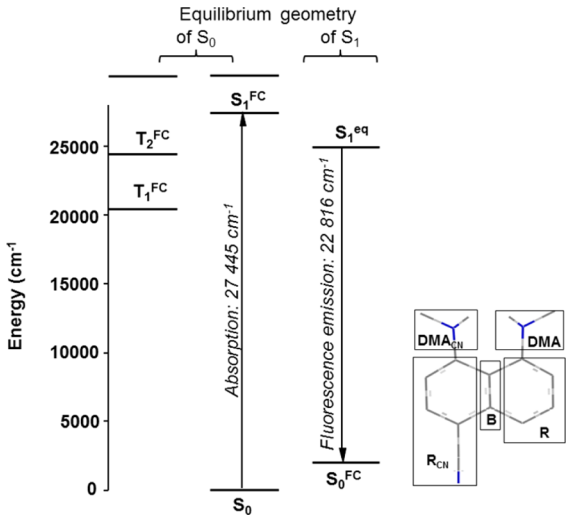

Figure 8. Jablonski diagram built from the low-energy singlet and triplet electronic states DMAN-CN. The singlet states S_0 and S_1^{FC} correspond to the equilibrium geometry of S_0, whereas S_0^{FC} and S_1^{eq} correspond to that of S_1. The energy calculations are performed at the TD DFT/B3LYP/6-31G(d,p) level. The inset at the right of the figure defines the chemical groups for which partial charges are given in Table 1.

Table 1. A Partial Charge Carried by the Chemical Groups Defined in the Inset of Figure 8

	S_0	S_1^{FC}	S_1	S_0^{FC}
DMA_{CN}	−0.1313	−0.0084	−0.1727	−0.1431
DMA	−0.1495	0.3696	0.1632	−0.0978
R_{CN}	−0.0063	−0.5900	−0.5571	−0.0397
R	0.1301	0.0193	0.3850	0.1230
B	0.1570	0.2094	0.1816	0.1575

Figure 8 is a Jablonski diagram showing calculated energies for the first singlet and triplet states of DMAN-CN. The energy of the states labeled S_0, $T_{1,2}^{FC}$, and S_1^{FC} in the figure were calculated at the equilibrium geometry of the ground state S_0, whereas S_1^{eq} and S_0^{FC} were calculated at that of S_1. The substantial stabilization revealed by the energy difference between S_1^{FC} and S_1^{eq} has its counterpart in the destabilization of the ground state, whose energy increases from 0 to the S_0^{FC}. As a result, even in the absence of any solvent, a quite large energy difference of 4629 cm^{-1} is expected between excitation and fluorescence. It is also interesting to observe in Figure 8 that the triplet states $T_{1,2}^{FC}$ are fairly close to S_1^{FC}. Hence, radiationless intersystem crossing (ISC) processes may become

DOI: 10.1021/acs.jpca.5b06631
J. Phys. Chem. A 2015, 119, 11233−11240

an efficient deactivation pathway at play when the S_1^{FC} state is relaxing and moves below the $T_{1,2}^{FC}$ states in a polar solvent. This was anticipated above to interpret that no fluorescence signal assigned to the CT state is observed in diethyl ether.

The inset in Figure 8 defines the chemical groups for which partial charges are listed in Table 1. From this table we know that the vertical excitation $S_0 \rightarrow S_1^{FC}$ promotes a large increase of the negative charge on R_{CN} (CN group + adjacent aromatic ring) at the expense of the DMAN-CN moiety which is not adjacent to the CN group. The excited-state relaxation ($S_1^{FC} \rightarrow S_1^{eq}$) leads to an additional flow of charge which makes the DMA_{CN} group substantially negative. Apparently, the CN group, which has the character of a strong electron attractor, affects all the chemical groups which are close to it. Note, however, that we must be very careful with the assignment of charges to specific groups of atoms since is does not rely on a well-defined quantum mechanical observable.

The additional charge migration upon the $S_1^{FC} \rightarrow S_1^{eq}$ relaxation shows up also when considering the dominant excitations which participate to the S_1 wave function. S_1^{FC}, i.e. the S_1 state at the ground state equilibrium geometry, is dominated by the HOMO−1→ LUMO and HOMO → LUMO excitations whereas S_1^{eq} is dominated by the single HOMO → LUMO excitation. The HOMO−1, HOMO, and LUMO orbitals are shown at these two geometries in Figure 3S.

To a large extent, the results found in the present work on DMAN-CN have similarities with those found in previous works on the DMAN.[16,17] In both molecules, the two DMA groups are twisted by the electronic excitation, and the emissive S_1 state gains a substantial CT character. However, due to the electron attractive character of the CN group, both S_0 and S_1 have a CT character that is substantially more pronounced in DMAN-CN than in DMAN. This shows up when considering the permanent dipole moment of these molecules. Upon the vertical $S_0 \rightarrow S_1^{FC}$ excitation, it increases indeed between 1.12 and 9.5 D in DMAN,[6] whereas its increase is between 7.08 and 17.08 D in DMAN-CN.[19]

3.7. Simulation of the Absorption Spectra of the Transient Species Populated Sequentially after Excitation of DMAN-CN in the S_1 State. The full analysis of the transient absorption spectra reported after excitation of DMAN-CN at 350 nm in *n*-hexane revealed that two transient species are populated sequentially by this excitation. The absorption spectra of these transient species appeared in Figure 6. The short-lived one was assigned to the absorption of S_1 when the electronically excited molecule has still the Franck−Condon geometry (S_1^{FC}) whereas the long-lived one would correspond to the absorption of S_1 from its equilibrium geometry (S_1^{eq}). These spectra can be simulated using the quantum chemistry calculations reported in the section above. However, the comparison between experiment and simulation is necessarily qualitative since the experiment is performed in a solvent whereas the calculation treats of isolated DMAN-CN. In particular, S_1^{eq} may not reflect exactly the same equilibrium geometry, and of course, the spectral shifts due to the solvent do not appear in the calculation.

Table 1S reports the calculated wavelengths and oscillator strengths of $S_1 \rightarrow S_n$ vertical transitions at two geometries of the molecule (S_1^{FC} and S_1^{eq}). This provides us with a stick absorption spectrum at each geometry, which is then convoluted by a Gaussian envelope (half-width of 900 cm^{-1}) to account for the experimental broadening.[29] The resulting spectra are shown in Figure 4S.

The absorption spectrum which was simulated at the Franck−Condon geometry (S_1^{FC} spectrum in Figure 4S) features two well-separated bands, below and above 570 nm. They peak at about 500 and 700 nm, respectively. Two such bands may be recognized in the light gray spectrum of Figure 6 which is associated with the transient species of short lifetime. Turning back to the simulated spectra, bands of similar location and shape are observed in the simulation performed at the equilibrium geometry of S_1 (S_1^{eq} spectrum in Figure 4S). Nevertheless, the bands are not as well separated as in the S_1^{FC} spectrum. Indeed, the simulated intensity does not go down to zero between the bands of the S_1^{eq} spectrum. The spectrum of Figure 6, associated with the long-lived species (black curve), may be reminiscent of the overlap between the bands of the S_1^{eq} in the simulated spectrum. The latter may be considered indeed as an unresolved double band, one peaking slightly below 500 nm and the other forming a long red wing broadly peaking at 700 nm. The relative intensity of the band is clearly not correct when comparing the S_1^{eq} simulated spectrum to the experimental black curve in Figure 6. This might be related to the fact that the calculations were performed on the isolated DMAN-CN molecule. The effect of solvation, even a nonpolar one as *n*-hexane, may not only shift the transitions wavelengths but also change the relative oscillator strengths of the transitions. Likely indeed, the final states in the $S_1 \rightarrow S_n$ ($3 \leq n \geq 15$) transitions do not have a comparable character either charge transfer or Rydberg.

4. CONCLUSIONS

The present work reports experimental and theoretical results concerning the dynamics of the DMAN-CN molecule in the S_1 state. On the experimental side, absorption, fluorescence, and time-resolved transient absorption spectra with a few hundred femtosecond resolution are provided when DMAN-CN is dissolved in various solvents: *n*-hexane, dodecane, and diethyl ether. The real-time dynamics (a few dozen femtosecond resolution) of this molecule was also studied in the gas phase. On the theoretical side, excited-state calculations were performed on this molecule at the TD DFT/6-31G(d,p) level, both at the equilibrium geometry of the ground state and at that of the S_1 state. The latter geometries were optimized at the CIS/6-31G(d,p) level. A consistent picture emerges from this double experimental and theoretical study, which can be summarized as the following scenario.

DMAN-CN has a strong absorption band, peaking near 350 nm, which corresponds to the $S_0 \rightarrow S_1$ transition. It can be assigned to the strongly absorbing ^1L_a state, actually S_1, in a geometry that is close to the Franck−Condon region of excitation, where it stays long enough to emit the blue band of the double band fluorescence spectrum which is observed in nonpolar solvents (*n*-hexane, dodecane). The calculations performed in the present work indicate that the ^1L_a state has a fairly strong charge transfer character. The gas-phase femtosecond pump−probe experiment which was unfortunately initiating the dynamics in the S_2 state instead of S_1 revealed a complex subpicosecond dynamics after the excitation, which is partly due to the spreading of the wavepacket within the S_1 potential energy surface in 500 ± 50 fs. The limited window at long time delays could not allow measuring the lifetime of the S_1 state after randomization of the wavepacket. The transient absorption spectra which were

DOI: 10.1021/acs.jpca.5b06631
J. Phys. Chem. A 2015, 119, 11233−11240

measured in *n*-hexane solutions after excitation of the S_1 state are consistent with the latter result. In a sequential picture of the evolution after electronic excitation of DMAN-CN at 350 nm, these results suggest that a transient species is populated by the electronic excitation. It decays with a time constant of 620 ± 50 fs into a second species of 251 ± 5 ps lifetime. The short-lived transient species with 620 ± 50 fs lifetime thus corresponds to the ^1L_a state mentioned above, and its lifetime appears as the time needed by the wavepacket to spread far outside the Franck−Condon region of excitation and reach a region of the S_1 potential energy surface where geometrical relaxation and solvent rearrangement have occurred. The latter corresponds to the CT state to which the species of 251 ± 5 ps lifetime is assigned. Compared to the ^1L_a state, we just saw that the CT state has experienced a substantial geometry relaxation, associated with a substantial reorganization of the solvent molecules.[30,31] Hence, fluorescence emission with a large Stokes shift is anticipated. This justifies that the CT state is responsible for the red-shifted emission band which is observed in the double band fluorescence spectra. The corresponding Stokes shift is about 13 500 cm^{-1} even in a nonpolar solvent like *n*-hexane. This value is similar to that observed for DMAN in the same solvent, and the two molecules, DMAN-CN and DMAN, are worth to be compared. The calculations show that in both of them the geometry relaxation is predominantly a twist of the DMA groups. Nevertheless, drastic differences exist since the lifetime of the CT state is measured to 251 ± 5 ps in DMAN-CN, whereas it was measured to ∼2.2 ns in DMAN.[16,17] Since the emission quantum yield of these molecules is very small (6×10^{-4} ± 10% and 1.4×10^{-3} ± 10% for DMAN-CN and DMAN, respectively), the lifetime of the CT state simply reflects the inverse of the rate of nonradiative processes. The latter is therefore a factor 8.8 larger in DMAN-CN than in DMAN. The presence of the cyano group on the 1,8-bis(dimethylamino)naphthalene skeleton has thus a profound influence on the excited-state dynamics of this class of molecules.

■ ASSOCIATED CONTENT

Supporting Information

The Supporting Information is available free of charge on the ACS Publications website at DOI: 10.1021/acs.jpca.5b06631.

Normalized absorption spectra of DMAN in *n*-hexane (a) and DMAN-CN in several solvents; calculated change of electronic charge distribution (Δ*Q*) in DMAN-CN on the excitation, relaxation, and fluorescence emission; decay of the time-correlated single photon counting detected emission of DMAN-CN in *n*-hexane; simulated transient absorption spectra of DMAN-CN (PDF)

■ AUTHOR INFORMATION

Corresponding Author

*Phone +48-71-3757366; e-mail anna.szemik@chem.uni.wroc.pl (A.S.-H.).

Notes

The authors declare no competing financial interest.

■ ACKNOWLEDGMENTS

We thank the Interdisciplinary Centre for Mathematical and Computational Modeling in Warsaw (Grant G32-10) and the Wrocław Center for Networking and Supercomputing (Grant nr 61) for the use of its computational facilities. The authors also thank Prof. Alexander F. Pozharskii (Rostov-on-Don State University, Russia) for providing us with the sample of DMAN-CN and M. Groeneveld from the University of Amsterdam for experimental assistance in femtosecond transient absorption experiments. Partial funding from LASERLAB-EUROPE (grant agreement no. 284464, EC's Seventh - Framework Program) is acknowledged.

■ REFERENCES

(1) Lippert, E.; Lüder, W.; Moll, F.; Nägele, W.; Boos, H.; Prigge, H.; Seibold-Blankenstein, I. Umwandlung von Elektronenanregungsenergie. *Angew. Chem.* **1961**, *73*, 695−706.

(2) Rettig, W. Charge Separation in Excited States of Decoupled Systems—TICT Compounds and Implications Regarding the Development of New Laser Dyes and the Primary Process of Vision and Photosynthesis. *Angew. Chem., Int. Ed. Engl.* **1986**, *25*, 971−988.

(3) Demeter, A.; Druzhinin, S.; George, M.; Haselbach, E.; Roulin, J.-L.; Zachariasse, K. A. Dual Fluorescence and Fast Intramolecular Charge Transfer with 4-(diisopropylamino) Benzonitrile in Alkane Solvent. *Chem. Phys. Lett.* **2000**, *323*, 351−360.

(4) Grabowski, Z. R.; Rotkiewicz, K.; Rettig, W. Structural Changes Accompanying Intramolecular Electron Transfer: Focus on Twisted Intramolecular Charge Transfer States and Structures. *Chem. Rev.* **2003**, *103*, 3899−4032.

(5) Hajj, V.; Louault, C.; Robert, M.; Saveant, J.-M. Concerted Proton Electron Transfers. Consistency between Electrochemical Kinetics and their Homogeneous Counterparts. *J. Am. Chem. Soc.* **2011**, *133*, 19160−19167.

(6) Kaila, V. R. I.; Hummer, G. Energetics of Direct and Water-Mediated Proton-Coupled Electron Transfer. *J. Am. Chem. Soc.* **2011**, *133*, 19040−19043.

(7) Edwards, S. J.; Soudackov, A. V.; Hammes-Schiffer, S. Analysis of Kinetic Isotope Effects for Proton-Coupled Electron Transfer Reactions. *J. Phys. Chem. A* **2009**, *113*, 2117−2126.

(8) Hoeben, F. J. M.; Jonkheijm, P.; Meijer, E. W.; Schenning, A. P. H. J. About Supramolecular Assemblies of p-Conjugated Systems. *Chem. Rev.* **2005**, *105*, 1491−1546.

(9) O'Neil, M. P.; Niemczyk, M. P.; Svec, W. A.; Gosztola, D.; Gaines, G. L., III; Wasielewski, M. R. Picosecond Optical Switching Based on Biphotonic Excitation of an Electron Donor-Acceptor-Donor Molecule. *Science* **1992**, *257*, 63−65.

(10) Bouit, P.-A.; Spnig, F.; Kuzmanich, G.; Krokos, E.; Oelsner, Ch.; Garcia-Garibay, M.-A.; Delgado, J.-L.; Martin, N.; Guldi, D. M. Efficient Utilization of Higher-Lying Excited States to Trigger Charge-Transfer Events. *Chem. - Eur. J.* **2010**, *16*, 9638−9645.

(11) Alder, R. W.; Bowman, P. S.; Steele, R. S.; Winterman, D. R. The Remarkable Basicity of 1,8-bis(dimethylamino)naphthalene. *Chem. Commun.* **1968**, *13*, 723−724.

(12) Petukhov, P. A.; Zhang, J.; Kozikowski, A. P.; Wang, C. Z.; Ye, Y. P.; Johnson, K. M.; Tella, S. R. SAR Studies of Piperidine-Based Analogues of Cocaine. 4. Effect of N-Modification and Ester Replacement. *J. Med. Chem.* **2002**, *45*, 3161−3170.

(13) Itoh, K.; Oderaotoshi, Y.; Kanemasa, S. Enantioselective Michael Addition Reactions of Malononitrile Catalyzed by Chiral Lewis Acid and Achiral Amine Catalysts. *Tetrahedron: Asymmetry* **2003**, *14*, 635−639.

(14) Shroff, R.; Svatoš, A. Proton Sponge: A Novel and Versatile MALDI Matrix for the Analysis of Metabolites Using Mass Spectrometry. *Anal. Chem.* **2009**, *81*, 7954−7959.

(15) Xiao, Y.; Fu, M.; Qian, X.; Cui, J. A Proton Sponge-Based Fluorescent Switch. *Tetrahedron Lett.* **2005**, *46*, 6289−6292.

(16) Szemik-Hojniak, A.; Balkowski, G.; Wurpel, G. W. H.; Herbich, J.; Van der Waals, J. H.; Buma, W. J. Photophysics of 1,8-Bis(dimethylamino)naphthalene in Solution: Internal Charge Transfer with a Twist. *J. Phys. Chem. A* **2004**, *108*, 10623−10631.

(17) Balkowski, G.; Szemik-Hojniak, A.; Van Stokkum, I. H. M.; Zhang, H.; Buma, W. J. Femtosecond Excited State Studies of the

DOI: 10.1021/acs.jpca.5b06631
J. Phys. Chem. A 2015, 119, 11233−11240

Two-Center Three-Electron Bond Driven Twisted Internal Charge Transfer Dynamics in 1,8-Bis(dimethylamino)naphthalene. *J. Phys. Chem. A* **2005**, *109*, 3535−3541.
(18) Kasha, M.; Rawls, H. R. Correlation of Orbital Classification of Molecular Electronic Transitions with Transition Mechanism: The Aromatic Amines. *Photochem. Photobiol.* **1968**, *7*, 561−569.
(19) Szemik-Hojniak, A.; Deperasińska, I.; Buma, W. J.; Balkowski, G.; Pozharskii, A. F.; Vistorobskii, N. V.; Allonas, X. The Asymmetric Nature of Charge Transfer States of the Cyano-Substituted Proton Sponge. *Chem. Phys. Lett.* **2005**, *401*, 189−195.
(20) Szemik-Hojniak, A.; Deperasińska, I.; Buma, W. J.; Balkowski, G.; Pozharskii, A. F.; Vistorobskii, N. V. Two Excited State Structures of Donor-Acceptor Substituted "Proton Sponge". *Key Eng. Mater.* **2005**, *277*−*279*, 1060−1065.
(21) Vistorobski, N. V.; Pozharskii, A. F. Peri-Naphthylenediamines. VII. Proton Sponge Aldehydes. *Russ. J. Org. Chem.* **1989**, *25*, 2154−2161.
(22) Vergeer, F. W.; Kleverlaan, C. J.; Stufkens, D. J. The First Steps of the Light-induced Biradical and Zwitterion Formation from the Clusters [Os3(CO)10(α-diimine)] Studied with Ultrafast Time-Resolved Absorption Spectroscopy. *Inorg. Chim. Acta* **2002**, *327*, 126−133.
(23) Sorgues, S.; Poisson, L.; Raffael, K.; Krim, L.; Soep, B.; Shafizadeh, N. Femtosecond Electronic Relaxation of Excited Metalloporphyrins in the Gas Phase. *J. Chem. Phys.* **2006**, *124*, 114302−114310.
(24) Eppink, A.; Parker, D. H. Velocity Map Imaging of Ions and Electrons Using Electrostatic Lenses: Application in Photoelectron and Photofragment Ion Imaging of Molecular Oxygen. *Rev. Sci. Instrum.* **1997**, *68*, 3477−3483.
(25) Frisch, M. J.;Trucks, G. W.; Schlegel, H. B.; Scuseria, G. E.; Robb, M. A.; Cheeseman, J. R.; Montgomery, J. A., Jr.; et al. *Gaussian 09, Revision B.01*; Gaussian, Inc.: Wallingford, CT, 2010.
(26) Van Stokkum, I. H. M.; Mullen, K. M. An R Package for Modeling Multi-way Spectroscopic Measurements. *J. Stat. Softw.* **2007**, *18*, 1−45.
(27) Noller, B.; Poisson, L.; Maksimenka, R.; Fischer, I.; Mestdagh, J.-M. Femtosecond Dynamics of Isolated Phenylcarbenes. *J. Am. Chem. Soc.* **2008**, *130*, 14908−14909.
(28) Poisson, L.; Nandi, D.; Soep, B.; Hochlaf, M.; Boggio-Pasqua, M.; Mestdagh, J.-M. A Roaming Wavepacket in the Dynamics of Electronically Excited 2-Hydroxypyridine. *Phys. Chem. Chem. Phys.* **2014**, *16*, 516−526.
(29) Caricato, M.; Trucks, G. W.; Frisch, M. J.; Wiberg, K. B. Oscillator Strength: How Does TDDFT Compare to EOM-CCSD? *J. Chem. Theory Comput.* **2011**, *7*, 456−466.
(30) Iwata, K.; Hamaguchi, H. Microscopic Mechanism of Solute−Solvent Energy Dissipation Probed by Picosecond Time-Resolved Raman Spectroscopy. *J. Phys. Chem. A* **1997**, *101*, 632−637.
(31) Owrutsky, J. C.; Raftery, D.; Hochstrasser, R. M. Vibrational Relaxation Dynamics in Solutions. *Annu. Rev. Phys. Chem.* **1994**, *45*, 519−555.

DOI: 10.1021/acs.jpca.5b06631
J. Phys. Chem. A 2015, 119, 11233−11240